Nano- to Microscale Dynamics of P-Selectin Detachment from Leukocyte Interfaces. I. Membrane Separation from the Cytoskeleton

Evan Evans,*†‡ Volkmar Heinrich,* Andrew Leung,† and Koji Kinoshita†
*Biomedical Engineering, Boston University, Boston, Massachusetts 02215 USA; and Departments of †Pathology and ‡Physics and Astronomy, University of British Columbia, Vancouver, British Columbia V6T 2B5, Canada

ABSTRACT We have used a biomembrane force probe decorated with P-selectin to form point attachments with PSGL-1 receptors on a human neutrophil (PMN) in a calcium-containing medium and then to quantify the forces experienced by the attachment during retraction of the PMN at fixed speed. From first touch to final detachment, the typical force history exhibited the following sequence of events: i), an initial linear-elastic displacement of the PMN surface, ii), an abrupt crossover to viscoplastic flow that signaled membrane separation from the interior cytoskeleton and the beginning of a membrane tether, and iii), the final detachment from the probe tip by usually one precipitous step of P-selectin:PSGL-1 dissociation. In this first article I, we focus on the initial elastic response and its termination by membrane separation from the cytoskeleton, initiating tether formation. Quantifying membrane unbinding forces for rates of loading (force/time) in the elastic regime from 240 pN/s to 38,000 pN/s, we discovered that the force distributions agreed well with the theory for kinetically limited failure of a weak bond. The kinetic rate for membrane unbinding was found to increase as an exponential function of the pulling force, characterized by an e-fold scale in force of ~17 pN and a preexponential factor, or apparent unstressed off rate, of ~1/s. The rheological properties of tether growth subsequent to the membrane unbinding events are presented in a companion article II.

INTRODUCTION

Bonds between the selectin family of adhesion receptors, e.g., P-selectin expressed on activated endothelial cells or platelets, and their glycosylated ligands, e.g., the leukocyte mucin P-selectin glycoprotein ligand 1 (PSGL-1), play a major role in the initial inflammatory response by interrupting the rapid transport of leukocytes in blood flow. The brief lifetimes of these bonds enable the cells to perform a rolling exploration of the vessel wall (Vestweber and Blanks, 1999; McEver, 2001). Recognized many years ago from studies of cells and receptor-bearing microspheres in flow chambers (Lawrence and Springer, 1991; Brunk and Hammer, 1997), the duration of the selectin adhesion bonds and their spacing along the wall (i.e., surface densities) are the principal determinants of the average cell rolling speed at a particular shear rate. Much more subtle, but also well known, the force exerted by hydrodynamic shear on an adhesive bond between the cell and the wall depends significantly on the lateral separation distance between the attachment site and the center of cell-surface contact (Kaplanski et al., 1993; Alon et al., 1995, 1997). Acting essentially as a lever or moment arm that reduces the force pulling on the adhesive bond, this distance often increases rapidly before detachment due to formation of a membrane nanotube, commonly referred to as a ''tether''. Easily extruded to lengths of several micrometers, membrane tethers have been shown to significantly impact the duration of PMN (human neutrophil) attachments and the dynamics of leukocyte rolling on PSGL-1 bearing substrates under conditions of flow (Schmidtke and Diamond, 2000; Park et al., 2002; Ramachandran et al., 2004).

Less well understood is the nanoscale mechanism leading to formation of a single membrane tether from the cell. Motivated by insights gained from mechanical studies of lipid bilayer vesicles (Božič et al., 1992; Evans and Yeung, 1994; Heinrich et al., 1999), it is often concluded that tether extrusion from cells begins at a yield force determined by the membrane bending stiffness and lateral tension in the cell plasma membrane. However, when the tether pulling forces are large, the membrane tension is postulated to reflect an energy of membrane adhesion per area of contact with the cytoskeleton (Hochmuth et al., 1996; Hwang and Waugh, 1997). By comparison to the onset of a lipid bilayer tether from a vesicle, Shao et al. (1998) observed a more complex scenario in their novel studies of single tether formation from PMNs. Using whole-cell aspiration into a large micropipette, they applied jumps in suction pressure to pull PMNs away from attachments to a monoclonal antibody-coated microsphere in a calcium-free medium. Observing a brief period of initial displacement into the pipette consistent with free motion of an unattached cell, they concluded that the attachments to PMN receptors had formed at the ends of floppy microvilli with an average length of ~300 nm. Also, tether growth was perceived to occur above a threshold in force, thought to depend on the ''degree of association between membrane and cytoskeleton,'' modeled in a subsequent article by an adhesion energy per area of membrane contact to the cytoskeleton (Marcus and Hochmuth, 2002). With the objective to examine single tether formation at much higher resolution and with biofunctional interactions that require divalent cations, we have used a high-resolution

Submitted August 23, 2004, and accepted for publication December 17, 2004.
Address reprint requests to Evan A. Evans, E-mail: evans@physics.ubc.ca.

0006-3495/05/03/2288/11 $2.00
doi: 10.1529/biophysj.104.051698

biomembrane force probe (BFP) to test P-selectin attachments to PSGL-1 on the PMN surface. In contrast to the earlier results (Shao et al., 1998; Marcus and Hochmuth, 2002), we will show that the onset of tether formation appears to be triggered by a molecular unbinding event within the membrane linkage to the PMN cytoskeleton, and that the separation of the membrane from the cytoskeleton nearly always occurs before P-selectin dissociation from PSGL-1. In the companion article II (Heinrich et al., 2005), we describe and analyze the rheology of the tether growth subsequent to the membrane-unbinding event over a broad range of pulling speeds from 0.4 to 150 μm/s. A third article III (King et al., 2005) presents simulations of the adhesive dynamics of a PMN under shear performed by our collaborators using the mechanical properties reported here for cell elasticity and in article II for tether rheology.

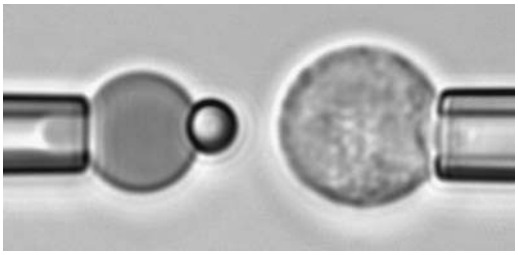

FIGURE 1 Video-micrograph of a biomembrane force probe (*left*) and a PMN leukocyte (*right*), both held by micropipette suction. Held stationary, the pipette-pressurized red blood cell (outer spherical diameter of ~6 μm) acted as the BFP force transducer. A P-selectin, and PEG-biotin, functionalized glass bead (~2 μm) was glued to the biotinylated red cell surface via streptavidin bonds as the BFP tip. To form and test P-selectin attachments, the PMN was driven to/from contact with the BFP tip using a closed-loop piezo translator coupled to the PMN-holding pipette.

MATERIALS AND METHODS

Biomembrane force probe: preparation, assembly, and operation

The methods used in the preparation of red blood cells for BFP force transducers and in the preparation of functionalized glass microspheres for BFP tips have been published previously (e.g., Evans et al., 2001). Briefly summarized, fresh samples of human red cells are collected, washed, and biotinylated by covalently linking an amine-reactive PEG-biotin polymer (NHS-PEG3400-biotin, Shearwater Polymers, Huntsville, AL) to their surface. The biotinylated red cells are then saturated with streptavidin (Sigma, St. Louis, MO) and washed for later assembly with a biotinylated glass bead. For attachment to a streptavidinated red cell as a BFP tip, borosilicate-glass microspheres (~2 μm diameter, Duke Scientific, Palo Alto, CA) are first cleaned in a mixture of ammonium hydroxide, hydrogen peroxide, and water at boiling temperature. After several washes in nanopure water, the glass beads are bound with mercaptosilane groups (mercaptopropyl-trimethoxy silane, United Chemical Technologies, Bristol, PA) and the beads are then baked in a clean drying oven to enhance the covalent attachment. For the experiments reported here, the silanized glass beads were reacted with a 4:1 mixture of maleimide-PEG3400-biotin plus malemeide-PEG3400-NHS (Shearwater Polymers) previously linked through amine reaction via the NHS group to monomeric P-selectin or the Fc-dimeric chimera of P-selectin (Glycotech, Rockville, MD). In the tests of P-selectin attachments to PMNs, a P-selectin decorated glass bead was attached to the red cell transducer by micromanipulation in a microscope chamber containing ~150 mOsm Hepes-buffered saline, pH 7.4, plus 1 mM calcium and 0.5% serum albumin (Hepes-calcium). To probe interactions with the β_2-integrin LFA-1 on PMNs, a soluble Fc-chimera of ICAM-1 (R & D Systems, Minneapolis, MN) was linked to the probe bead via the NHS functional group instead of P-selectin and 2 mM magnesium was used in the buffer instead of calcium. In addition, the PMNs were washed in a EDTA plus EGTA buffer, then washed and resuspended in the magnesium containing buffer for the tests.

Assembly of the BFP requires carefully maneuvering of the biotin- and protein- functionalized microsphere into axisymmetric alignment with the streptavidinated (PEG-biotinylated) red cell transducer, which is held by micropipette suction and pressurized into a spherical shape. Once aligned, the microsphere is pushed against the red cell transducer, forming a strong adhesive contact and producing the BFP assembly shown on the left in Fig. 1. Prevented from adhesion to the glass tube by coating with albumin, and pressurized into a smooth sphere, the membrane tension $\underline{\sigma}$ becomes uniform over the entire surface of the red cell transducer. A hypotonic buffer (150 mOsm) is used in the test chamber to swell the red cell, thereby reducing its aspiration length and preventing formation of a membrane crease when pulled tight into the micropipette. From mechanics, the level of tension is readily shown to be proportional to the aspiration pressure Δp and the pipette radius R_p, with a secondary dependence on the radius R_0 of the outer-spherical portion of the cell,

$$\underline{\sigma} = \frac{1}{2}\frac{R_p}{(1 - R_p/R_0)}\,\Delta p. \tag{1}$$

When extended or compressed along its axis of cylindrical symmetry, the outer portion of the cell deviates from a sphere, and for small displacements, the changes in axial length have been shown to be directly proportional to the axial force (Evans et al., 1995). As such, the red cell capsule behaves like a Hookean spring, and its spring constant k_f for small deflections is governed mainly by membrane tension,

$$k_f \cong 2\pi\frac{\underline{\sigma}}{\ln\left[4R_0^2/(R_p r_c)\right]}, \tag{2}$$

but also involves a weak logarithmic dependence on the characteristic dimensions (R_0, R_p) of the cell and pipette, as well as the radius r_c of the adhesive contact between the glass bead and cell. Thus, the BFP spring constant can be accurately adjusted over a wide range (~0.2–2 pN/nm) by simply changing the pipette suction pressure, which has been verified experimentally (Evans et al., 1995; Simson et al., 1998). Without further calibration, the accuracy is essentially determined to ~5–10% (as for membrane tension) by the measurements of the pipette radius and the cell outer dimension. Multiplied by the spring constant k_f, the displacement of the glass bead along the axis provides the force applied in pulling or pushing on the BFP tip.

To quantify the BFP force, we have developed a high-resolution method of video image analysis for tracking the dark diffraction band at the rear of the glass bead. Incorporated into a complete system, the instrument combines an inverted optical microscope (Carl Zeiss, Thornwood, NY) with fast video image processing using a high-speed digital camera (SensiCam, Cooke, Auburn Hills, MI). Binning and digitizing a set of video lines along the symmetry axis of the probe at a scan rate of 1500/s (50-fold faster than the conventional video framing speed of 30 fps), displacements of the BFP tip and target bead are tracked along the pulling direction at time intervals of ~0.0006 s and at a resolution of ~±5 nm. The BFP tip displacement is multiplied by the spring constant k_f to give the force at each time. With online feedback control of the linear piezo translator connected to the PMN-holding pipette, computer software is used to control the approach of the test surface (here a PMN) to the BFP tip, the impingement force and duration of

the initial touch to the probe, and the retraction speed of the test surface following touch. Under very fast deflections of the BFP transducer, the force reported by the transducer must be corrected for viscous damping. As reported previously (Evans et al., 2001), a constant damping coefficient ($\zeta_{BFP} \sim 0.0005$ pN s/nm) has been found to characterize the response of the transducer, based on measurements of the viscoelastic recovery at different settings of the BFP spring constant.

Testing attachments to native and latrunculin-treated human PMNs

White blood cells were obtained from a small finger prick drop of blood diluted in a large volume of the 150 mOsm Hepes-calcium buffer. In the hypotonic environment, the PMNs first swelled and then, given a few minutes to equilibrate, the cells resumed a size (8.6 ± 0.2 μm, in 150 mOsm buffer) very close to that in isotonic buffer (8.3 ± 0.2 μm, in 300 mOsm buffer) through osmotic regulation. After preequilibration, and assayed by micropipette aspiration, the PMNs in the hypotonic medium exhibited nearly the same turgor pressure and whole cell deformability, both governed by an apparent cortical tension (0.03 ± 0.006 mN/m, in 150 mOsm buffer + 1 mM calcium), as for PMNs in isotonic conditions (0.02 ± 0.004 mN/m, in 300 mOsm buffer, no calcium). An aliquot of this suspension was deposited into a separate holding chamber and placed on the microscope stage. At the start of each measurement, a PMN was selected by a micropipette, transferred into the adjacent BFP test chamber and held while the BFP was being assembled. Once arranged as shown in Fig. 1, the PMN holding pipette was translated repeatedly to/from BFP contact with better-than nanometer accuracy using a closed-loop piezo actuator (Polytec PI, Auburn, MA). Typically, a new BFP (fresh red cell plus probe bead) was assembled and used with a fresh PMN after a few hundred test cycles. In the course of each experiment, the suction applied to the PMN was kept as low as possible while still maintaining the cell stable throughout the manipulation procedure.

To destabilize the F-actin network, PMNs were preincubated for 15 min in a Hepes buffer that contained 1 μM concentration of the cytotoxic drug latrunculin A (Molecular Probes, Eugene, OR). An aliquot of the pretreated cells were then introduced into the microscope holding chamber. Because the effects of latrunculin are reversible, both the holding and test chambers also contained latrunculin A.

Controls for specific ligand attachment and nonspecific hydrodynamic forces

As the first control for P-selectin specificity, PMNs were tested against P-selectin tips in a calcium-free Hepes buffer that contained 10 mM EDTA. When checked under slow-to-moderate retraction speeds (<10 μm/s), the frequency of PMN attachments fell from levels of ~35–70/100 touches in Hepes-calcium to ~2–4/100 touches in Hepes-EDTA, and the few forces detected in EDTA were very small. As a second control, the P-selectin tip was replaced by an albumin-linked tip and tested against PMNs in Hepes-calcium at slow-to-moderate retraction speeds. Here, an even bigger drop was observed in the attachment frequency than in the tests with Hepes plus EDTA. Together, the two controls verified that nearly all attachments in the functional tests with calcium were held by P-selectin bonds. Similar controls were performed to verify specificity between PMNs and probe tips functionalized with ICAM-1.

In regard to nonspecific forces, it is important to note that very fast retraction of PMNs (>50 μm/s) in the control tests always produced high frequencies of apparent attachments due to a speed-dependent hydrodynamic ''suction'' between the probe tip and the soft PMN surface. This type of nonspecific force is unavoidable when attempting to probe soft cell surfaces at fast loading rates ($>10^4$ pN/s). The nonspecific suction force arises from the well-known ''Reynolds lubrication'' effect where viscous dissipation dramatically impedes the flow of aqueous fluid into the narrow gap between the cell surface and probe tip. As such, these forces can vary significantly depending on the impingement area, and on the cell-surface deformability and roughness. In the case of pulling PMNs away from nonspecific protein-decorated BFP tips, the magnitude of nonspecific hydrodynamic suction forces was found to become significant when retraction speeds exceeded 25 μm/s, contributing forces from 0 to ~15–25 pN at 25 μm/s and from 0 to ~50–70 pN at retraction speeds of 150 μm/s. Obtained using albumin and PEG functionalized tips, distributions of these nonspecific forces are compared in Fig. 2 with the range of forces obtained for membrane-cytoskeletal unbinding events at fast speeds. Fortunately, when pulling on the cell at a point, this type of hydrodynamic coupling falls rapidly because local deflection of the cell surface enables the opening of a large initial lubrication gap and quickly allows the cell surface to separate from the probe tip. As illustrated in Fig. 2, the forces characterizing separation of the membrane from the cytoskeleton and the subsequent dynamics of tether formation were well beyond the range of nonspecific forces even at ultrafast separation speeds.

RESULTS

In testing hundreds of point attachments to nearly 60 different PMNs, we used BFP tips linked with both monomeric P-selectin and a dimeric Fc chimera of P-selectin. Touches to PMNs with these tips produced 30–70% attachments, depending on the concentration and type of P-selectin used in the tip preparation. Qualitatively, the majority of attachments to PMNs with both the mono- and dimeric P-selectin tips exhibited the same type of force history up to final detachment from the tip, appearing to reflect a single molecular site of attachment. Still, because two-thirds of the tests were performed with the Fc chimera of P-selectin and half of these tips had P-selectin concentrations sufficient to

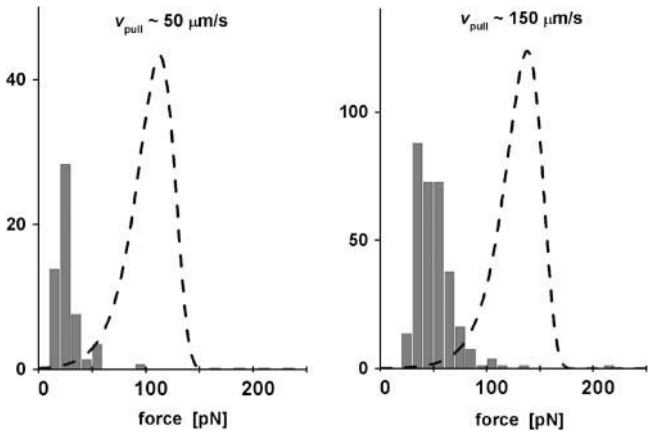

FIGURE 2 Histograms of nonspecific hydrodynamic suction forces (*shaded* bins) measured when pulling PMNs away at fast speeds following ~10 pN touch to a nonspecific BFP tip. Here, the tip was an albumin and PEG-biotin functionalized glass bead. Frequencies of apparent nonspecific attachments with this tip were <2% at pulling speeds ≤10 μm/s, but rose to ~40% at pulling speeds of 50 μm/s and >60% at 150 μm/s. Normalized by the frequencies of specific attachment to P-selectin tips, the dashed curves are the force ranges characterizing membrane unbinding from the PMN cytoskeleton at these pulling speeds (taken from Fig. 7).

produce attachments in 60–70% of touches, a few tests of attachments showed obvious features of multiple-point attachments and multiple steps of P-selectin release as briefly described in article II (Heinrich et al., 2005). Here, we will only consider the large fraction (79%) of tests that appeared to end in a single step of P-selectin:PMN detachment. Thus, we expect the force histories from these tests to primarily represent the responses of attachments to single P-selectin sites on the probe tip.

Fig. 3 presents a schematic of the BFP spring response and the associated PMN deformation that occurred during a typical cycle of approach, impingement (touch) against the P-selectin tip, and retraction at speeds ≥ 1 μm/s. Fig. 4 shows examples of the force-time plots (histories) obtained while pulling on attachments at slow and fast retraction speeds. As sketched in the lower panels of Fig. 3, tensile loading of the PMN attachment began with a nanoscale elastic extension of the PMN that was interrupted by the onset of membrane tether growth and ended with the recoil of the BFP at the moment of P-selectin release. Demonstrated explicitly in Fig. 4, two regimes of force response appear in the retraction phase, distinguished by the abrupt termination of an initial linear rise in force at a crossover point (labeled $f_{\otimes}$) and followed by a noticeable slowing of the increase in force with approach toward a plateau (labeled f_{∞}). Examining the initial elastic-like regime of PMN extension, we will first determine the loading rate r_f (force/time) and the stiffness coefficient k_i (pN/nm) that characterize the initial cell deformation when pulling on the point attachment. Next, collecting the crossover (yield) forces $f_{\otimes}$ at the termination of the elastic regimes into histograms at the various loading rates r_f, we will show that the force distributions agree with the probability densities predicted by the kinetics of a specific molecular failure event occurring under different ramps of force.

Initial elastic extension of the PMN under a point load

When retracted at a constant speed v_{pull}, the total displacement of the PMN was specified by the product of retraction speed and time. This displacement included the extension of the PMN (Δx_{cell}) and the deflection of the transducer [$\Delta x_f = f(t) / k_f$] produced by the attachment force $f(t)$, i.e., $v_{pull}\, t = \Delta x_{cell} + \Delta x_f$. Because the pulling speed and BFP stiffness were fixed, the initial linear rise in force with time revealed that the PMN deformation also increased in linear proportion to force over this period, consistent with an elastic-like response. The elastic stiffness of the initial PMN extension (labeled k_i) was derived from the ratio of the nominal force-loading rate, $r_f^o = k_f\, v_{pull}$, to the measured loading rate, $r_f = \Delta f / \Delta t$ (slope of the initial regime), using the expression, $k_i = k_f/(r_f^o/r_f - 1)$, which follows from the stretch of two linear springs in series. The large reduction in loading rate from the nominal value revealed a very soft elastic stiffness for local extension of the PMN under a point load. Cumulated in Fig. 5 *A* as a function of the rates of initial cell extension, $\Delta x_i / \Delta t = r_f / k_i$, the values of PMN stiffness were obtained from analysis of several thousand PMN attachments over a range of pulling speeds from 0.4 to 150 μm/s. As seen in Fig. 5 *A*, the local elastic stiffness seems to depend very weakly on the rate of surface deformation, i.e., $\sim(v_{pull})^{0.07}$, which was not detected in the limited period of linear cell deformation at each rate. As we discuss later, a likely source for this weak dependence on pulling speed is the slow viscoelastic response of the whole cell body that

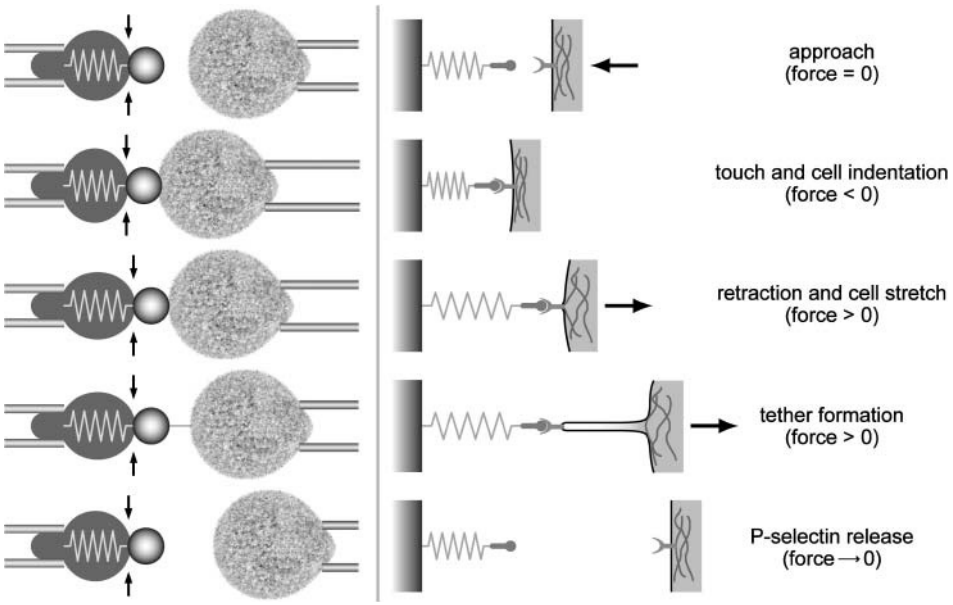

FIGURE 3 (*Left*) Schematic of the PMN approach-touch-retraction to/from the BFP tip accompanied by a point attachment to the P-selectin tip. (*Right*) Compression and extension of the ''spring'' illustrate the typical BFP response at each step of the test. The adjacent ''material slices'' show the sequence of PMN surface deformations associated with the spring response: i), elastic compression of the cortical cytoskeleton at touch and ii), stretch on retraction; iii), membrane separation from the cytoskeleton and the onset of a membrane tether; and iv), membrane recovery after P-selectin detachment.

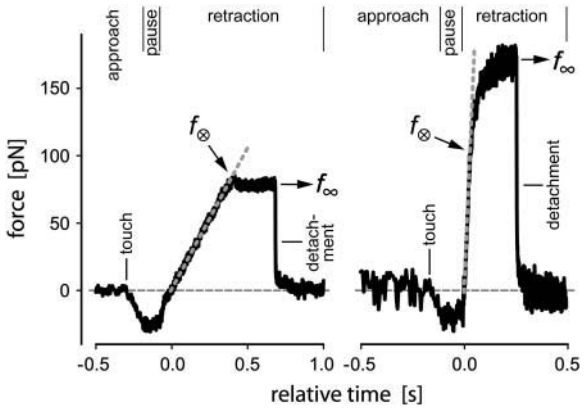

FIGURE 4 Examples of BFP force-time curves obtained over the course of PMN detachment at slow (~2 μm/s) and fast (~50 μm/s) retraction speeds. Controlled by piezo translation of the PMN-holding pipette, the periods of approach, touch, and retraction are noted at the top of the figure. The final precipitous drop in force shows the BFP recoil upon cell-surface detachment from the P-selectin tip. The crossover force $f_\otimes$ marks the abrupt termination of the linear elastic deformation of the PMN surface and the onset of tether flow. Beyond the crossover, the increase in force slows noticeably to approach a speed-dependent plateau f_∞. (Note that, when compared to the force curve at slow retraction speed, the larger force noise in the force curve at the fast speed stems from a threefold larger value of BFP spring constant.)

accompanies the initial elastic extension but proceeds over much longer time frames ($\geq$1 s).

Impact of the receptor type on the PMN extension and the crossover to tether formation

To confirm that the initial PMN elasticity was a property of the cell cytoskeleton and independent of the type of adhesion receptor, we also analyzed the local PMN extension obtained by pulling on point attachments to the integrin LFA-1 activated by Mg^{2+} or Mn^{2+} using a probe functionalized with recombinant ICAM-1 Fc. The cumulated results for the local PMN stiffnesses obtained by pulling on LFA-1 are included with the results from pulling on PSGL-1 in Fig. 5 *A*. The close similarity in local stiffness is also clearly demonstrated by the near-perfect coincidence of two force-time curves obtained from pulling on PSGL-1 and LFA-1 in separate PMN tests (cf. Fig. 5 *B*). However, unlike attachments to PSGL-1 on the PMN surface, the ICAM-1 ligand nearly always (>95%) dissociated from the activated integrin before a tether could form. (As an additional comparison, we have included results obtained from pulling on L-selectin with a PSGL-1 functionalized probe in Fig. 5 *A*.)

Initial elastic stiffness of the PMN under local compression

Complementary to the extensional stiffness in pulling, we also evaluated the stiffness coefficient for compression of the PMN interface from analysis of the force/indentation response during touch to the BFP tip. Although not analyzed in detail, these results are briefly summarized in Appendix I. The effective compressional stiffness of the PMN in 1 mM Mg^{2+} was found to be of comparable magnitude (k_{comp} ~ 0.2–0.3 pN/nm) to the extensional stiffnesses plotted in Fig. 5 *A* for pulling at a point. The similarity between elastic stiffness for initial compression or extension is intriguing, although much work would be needed to pin down its mechanical origin. In regard to local elastic stiffness, there are two obvious possibilities to consider. The first is that the stiffness characterizes deflection of a thin tension-bearing interface, following an expression like that for the BFP force constant. Based on aspirations of PMNs into a pipette, it's been known for some time that the large-scale elastic deformations of a PMN seem to be dominated by a cortical tension (Evans and Yeung, 1989). As noted in the Materials and Methods section, this apparent tension is usually small, e.g., ~0.03 mN/m for the experiments here with 1 mM calcium, and is unlikely to be the principal determinant of either local elastic stiffness, k_i or k_{comp}. On the other hand, k_i and k_{comp} could reflect bending rigidity of the cortex. In order for the stiffnesses in compression and extension to be

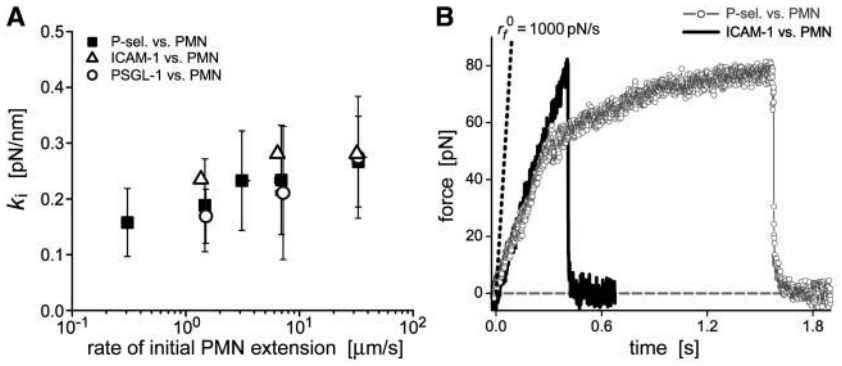

FIGURE 5 (*A*) Stiffnesses k_i for the initial elastic-like extension of PMNs measured under point loading over a range of pulling speeds from 0.4 to 150 μm/s. The results are plotted as a function of the rates of PMN-surface extension, $\Delta x_i / \Delta t$. Shown along with the results for P-selectin attachments (*solid squares* bracketed by $\pm$ SD) are values for the mean stiffness measured under point loading of ICAM-1 attachments to LFA-1 integrin in Mg^{2+} (*open triangles*; K. Kinoshita, A. Leung, V. Heinrich, S. Simon, and E. Evans, unpublished data) and values for point loading of PSGL-1 attachments to L-selectin (*open circles*). (*B*) Force-time curves obtained by pulling on attachments to PSGL-1 on a PMN in Ca^{2+} (*gray open circles*) and to LFA-1 on a PMN in Mg^{2+} (*black solid line*) using identical pulling speeds of 2 μm/s and BFP spring constants of 0.5 pN/nm. Although both types of attachments exhibit the same initial linear deformation of the PMN surface, pulling on ICAM-1 ended with abrupt dissociation from the integrin and no tether formation.

comparable, we know from the mechanics of shells (Landau and Lifshitz, 1986) that the rigidity constant k_{bend} would have to exceed the product of the indentation or pulling force f and the dimension scale d_c over which the force is applied, more specifically given by the inequality, $k_{bend} > f\,d_c/2\pi$. If so, there would be little difference between the elastic response for pulling at a point or for indenting over a small area of bead contact. Based on the data for PMN compression, the bending rigidity $\underline{k}_{bend}$ would need to be $\sim$10 pN μm or greater to account for both k_i and k_{comp}. This level of bending rigidity would be equivalent to a small Young's modulus of $\sim 10^2$ N/m^2, assuming a 1-μm-thick cortex. Interestingly, the shear modulus measured for F-actin is of comparable magnitude at concentrations likely to exist in the PMN cortex (Janmey et al., 1988, 1991).

Impact of latrunculin on the PMN elastic extension and crossover to tether formation

The abrupt transition between an initial elastic-like displacement and the onset of plastic-like flow at the crossover force $f_\otimes$ signaled separation of the membrane from the interior cytostructure. To test the impact of cytoskeletal cohesion on this separation force, we examined P-selectin attachments to PMNs in Hepes-calcium containing 1 μM of the cytotoxic drug latrunculin A, which is known to bind actin monomers and inhibit F-actin polymerization. As demonstrated in Fig. 6, treatment with latrunculin produced a dramatic reduction in the force for membrane separation, and the plastic regime of tether formation seemed to begin almost immediately under tensile loading. Thus, the existence of an elastic-like regime, and the large force needed for membrane separation from the cytoskeleton, required an intact F-actin network.

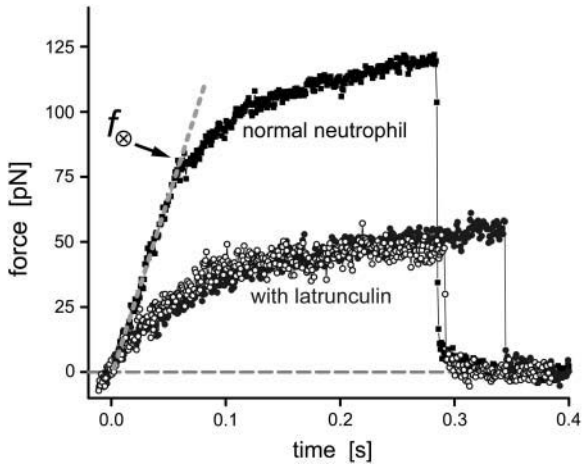

FIGURE 6 Comparison of force-time curves obtained from pulling on a P-selectin attachment to a PMN in Hepes-calcium buffer (*solid squares*) and from pulling on two different P-selectin attachments to a PMN in the same buffer containing 1 μM latrunculin A (*solid and open circles*). In the presence of latrunculin, the initial linear elastic deformation of the PMN disappeared and the plastic process of tether growth seemed to begin near zero force. Both tests were performed at the same nominal loading rate of $r_f^o = 5000$ pN/s and pulling speed of 10 μm/s.

Kinetically limited failure of the membrane linkage to the PMN cytoskeleton

Given the high probability of a single PSGL-1 attachment site, it seemed likely that the abrupt termination of the elastic-like regime at the force $f_\otimes$ originated from a molecular unbinding event within the membrane-cytoskeletal linkage local to the PSGL-1 receptor and that this failure event enabled membrane separation. To examine this hypothesis, we collected the crossover forces for membrane separation from thousands of tests at pulling speeds from 0.4 to 150 μm/s, establishing histograms over a 200-fold range of initial elastic loading rates r_f from 200 pN/s to 40,000 pN/s. Examples of the force histograms are shown in Fig. 7 *A* for four pulling speeds between 2 and 150 μm/s. Summarizing all of the data, the mean yield forces ($\pm$ SD) are plotted in Fig. 7 *B* as a function of the logarithm of the mean loading rates r_f ($\pm$ SD) measured in the elastic regimes. The statistics of membrane separation forces as a function of loading rates provide the basis for comparison to a simple kinetic model for dynamic failure of a weak chemical bond.

The model for bond rupture is based on the physical idealization that the application of a tensile force to a bond dramatically increases the off rate (failure rate) by lowering the free energy barrier impeding bond dissociation. Assuming that passage of the barrier contributes a fixed length x_β in the direction of force, the consequence of pulling on a bond is a failure rate that increases exponentially with force, $k_{unbind}(f) \approx (1/t_o)\exp(f/f_\beta)$, following the original postulate by Bell (1978). The e-fold scale f_β is the level of force needed to lower the free energy barrier by one unit of thermal energy, i.e., $f_\beta = k_BT / x_\beta$. Under conditions of steady loading (r_f = constant) as over the initial elastic regime of PMN extension, the distributions of unbinding forces are predicted to exhibit identical shapes at all loading rates while shifting progressively to higher forces in proportion to the logarithm of loading rate (Evans and Ritchie, 1997; Evans and Williams, 2002). The generic function, $p(y) \sim \exp[y - \exp(y)]$, specifies the force distribution $p(f)$ at each loading rate r_f through the parameterization given by, $y = f/f_\beta - \ln(r_f\,t_o/f_\beta)$. Thus, the crucial indicator for kinetically limited failure of a single bond is agreement between the histograms of rupture forces measured over a large span in loading rate and the probability density distributions computed with a common set of the bond kinetic parameters, f_β, t_o.

Revealing the key dynamic feature of this model for bond rupture, the forces at failure should increase in proportion to the logarithm of the applied loading rate, as given by the most frequent rupture force, $f^* = f_\beta \ln(r_f\,t_o/f_\beta)$. This simple expression provides the starting point for analysis of the data, after which the probability distributions are readily computed. Thus, we begin by examining the plot of mean

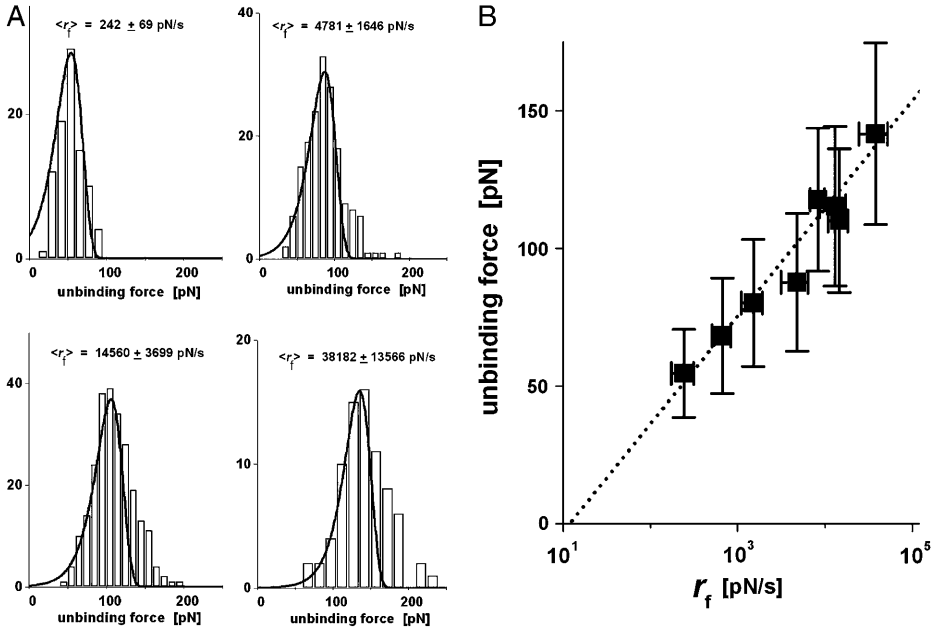

FIGURE 7 (*A*) Sample histograms of the forces $f_{\otimes}$ for membrane unbinding from the cell cytostructure. Obtained from the linear fits to initial elastic regimes at four pulling speeds from 2 to 150 μm/s, the mean loading rates r_f ($\pm$ SD) are given at the top of each histogram for each pulling speed. Superposed on the distributions are the probability densities (*solid curves*) modeled by the theory for kinetically limited failure of a single bond, given a failure rate that increases exponentially with pulling force according to the relation, $k_{unbind}(f) \approx (0.7–1.7/s)\ \exp(f / 17\ pN)$. (*B*) The mean values (*solid squares*, $\pm$ SD) of membrane unbinding force measured at pulling speeds from 2 to 150 μm/s are plotted versus the logarithms of the mean loading rates ($\pm$ SD) to demonstrate the full range of experimental data. The slope of the dashed-line fit (17 pN) was used to define the force scale for exponentiation of the failure rate.

forces as a function of the logarithm of the mean loading rates r_f in Fig. 7 *B*. As shown by the linear regression in Fig. 7 *B*, the forces increase steadily as expected for kinetically limited failure, with the slope indicating a thermal force scale of $f_\beta \approx 17 \pm 1$ pN. (Note that, at force levels above twice the thermal scale f_β, the means of force distributions closely follow a linear dependence on the logarithm of loading rate. However, due to the asymmetric shape of the generic distribution, the mean values are given by $\langle f \rangle \approx f_\beta \ln(0.56\ r_f\ t_o / f_\beta)$). To verify the kinetically limited behavior implied by the dashed line in Fig. 7 *B*, we fixed the force scale at $f_\beta = 17$ pN and matched the theoretical probability distribution to the force histogram at each loading rate, treating the unstressed failure rate $1/t_o$ as a fitting parameter to account for the significant cell-to-cell variations in the loading rate. As demonstrated by the examples in Fig. 7 *A*, the theoretical distributions were found to closely match the histograms at all loading rates, restricting the unstressed failure rates to a narrow range, $1/t_o = 0.7–1.7$/s. The small wings of forces beyond the predicted distributions in Fig. 7 *A* can be accounted for by assuming a few (<20%) double linkages to the cytoskeleton. Hence, the analysis of the distributions of forces for membrane separation implies that the strength of the membrane linkage to the cell cytostructure is regulated by a weak chemical bond whose rate of failure increases exponentially under force as described by, $k_{unbind}(f) \approx (0.7–1.7/s)\ \exp(f / 17\ pN)$.

CONCLUSIONS

Retracting PMNs at speeds between 1–150 μm/s from point attachments to a BFP decorated with P-selectin, we have observed a common force response, characterized by two distinct regimes of PMN material behavior. In the first regime, the force increased linearly with time, indicating an initial elastic deformation of the cell. Then, an abrupt drop in the rate of force increase marked the end of the elastic regime and signaled the crossover to a second viscous-like regime where membrane tether flow ensued. Measuring the forces and displacements at high resolution, we found that the linear elastic response to a positive-tensile load on the P-selectin attachment covered distances up to 200–500 nm, yielding a stiffness coefficient between 0.2 and 0.3 pN/nm. However, we failed to detect the long ''natural'' microvillus length reported by Shao et al. (1998). Sensing contact to the PMN surface at forces of ~1 pN, our measurements show that the soft roughness of the PMN interface seems not to extend beyond 10 nm. On the other hand, as demonstrated in Appendix II, the initial elastic PMN deformations measured here would appear as the same ''free motion'' displacement attributed to a natural microvillus length in the whole-cell aspiration experiments of Shao et al. (1998). Also demonstrated in Appendix II, the large apparent stretch of microvilli described in Shao et al. (1998) seems most likely to have arisen from a slow viscous elongation of the cell body on a longer timescale of ~1 s. Only significant well beyond the onset of tether formation, the cell-body extension was not quantified in our experiments, but we show that this slow elongation can account for the weak apparent dependence of the initial elastic stiffness on pulling speed seen in Fig. 5 *A*. Separation of the membrane from the cell cytostructure triggered tether formation, nearly always preceding dissociation of the P-selectin adhesive bond. As we demonstrate in article II (Heinrich et al., 2005), membrane separation from the cytoskeleton seemed to act like a mechanical fuse limiting the force, enabling a longer duration of attachment

to a PMN. By comparison, pulling on ICAM-1 attachments to LFA-1 nearly always resulted in ICAM-1 release from the integrin before a tether could form. Treating the PMNs with latrunculin A seemed to eliminate the elastic regime and enabled tether initiation close to zero force.

Analyzing the histograms of forces characterizing membrane separation from the cytoskeleton, we have shown that the distributions agree with the kinetic model for failure of a single molecular bond, where the kinetic rate of failure increases as an exponential function of the force. From correlation of the single-bond model to the force histograms obtained at all pulling speeds, we find that the kinetic rate for membrane unbinding from the cytoskeleton is characterized by an apparent unstressed prefactor of $\sim 0.7-1.7$/s, from which the rate rises exponentially with pulling force on a scale of $\sim 17 \pm 1$ pN (equivalent to gaining a length of ~ 0.24 nm at bond dissociation). Both the elastic regime, and the membrane anchoring force, appeared to vanish in the presence of latrunculin A, demonstrating that the strength of the membrane linkage to the cell cytostructure requires an intact network of F-actin. In the case of attachments to PSGL-1, there seem to be two likely candidates for a locus of failure in the membrane linkage to the cytoskeleton. The first would be somewhere in the nearby F-actin network, and the other would be in the complex of ERM (ezrin/radixin/moesin) proteins required for linkage of PSGL-1 tail domains to F-actin (Mangeat et al., 1999; Urzainqui et al., 2002; Serrador et al., 2002; Snapp et al., 2002). Less obvious, other specific molecular interactions between the membrane and cytoskeleton could be involved. However, it is very unlikely that a multiplicity of interactions could produce the clear signature of single-bond kinetics seen in Fig. 7. Using cell transfectants with strategic receptor tail-splice variants or knock outs of specific actin binding proteins, the high-resolution technique reported here can provide a powerful quantitative method to explore the chemical factors governing linkage of PSGL-1 and other transmembrane receptors to the cell cytoskeleton.

APPENDIX I: ELASTIC STIFFNESS FOR PMN INDENTATION

Before testing P-selectin attachments to PMNs under steady speed retraction, we first used the BFP with a nonspecific tip to evaluate the mechanical resistance to indentation or ''flattening'' of the cell in calcium-free media. The first experiments were performed in Hepes buffer without calcium so that the cells could be probed many times without forming pseudopodia. Several cells were tested and each was indented many times through repeated cycles of PMN touch to the BFP. The results are shown in Fig. A1 (*left*). The first tests of PMN indentation were performed using large probe tips of 3.5 ± 0.05 μm diameter and are labeled in Fig. A1 (*left*) according to the particular cycle (e.g., cycle 5 = force/indentation for the fifth touch). A common linear resistance to compression was found for the initial phase of indentation in all cycles of touch to a PMN surface, yielding a stiffness coefficient, $k_{comp} \approx 0.147$ pN/nm (linear regression shown in Fig. A1). The surprising outcome in the absence of divalent cations was that repeated touches to the cells led to a progressive stiffening in the cell cortex.

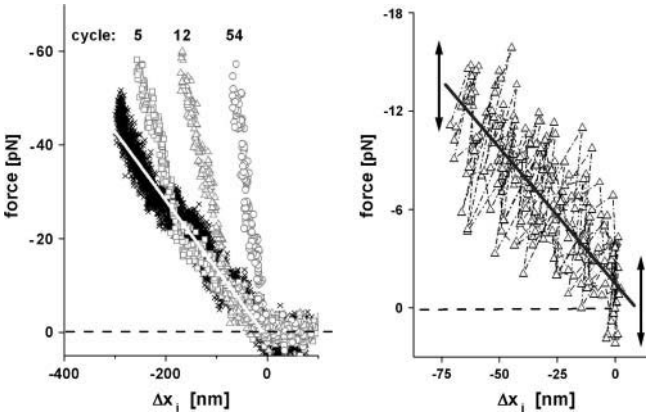

FIGURE A1 PMN surface indentation in the absence of divalent cations. (*Left*) Data of force versus indentation distance measured with large diameter probe tips, 3.5 ± 0.05 μm. (*Right*) Data of force versus indentation distance measured with small diameter probe tips, 2.3 ± 0.08 μm. The mean stiffnesses derived for indentation of the PMN interface are $k_{comp} = 0.15$ and 0.16 pN/nm respectively. The double-ended arrows in the right figure illustrate the expected resolution in force set by a probe spring constant of 0.5 pN/nm and $\sim \pm 5$ nm errors in the tracking of bead displacements.

Revealed by the marked upward shift in slope after some compression distance, the cortical stiffening reached a maximum after ~ 50 indentations. Within the measurement error, the linear resistance to PMN compression appeared to commence at contact. Similarly, although covering a smaller range of compression at lower levels of force, the results for indentation with smaller tips of 2.3 ± 0.08 μm diameter (shown in Fig. A1, *right*) gave nearly the same stiffness coefficient, $k_{comp} \approx 0.16$ pN/nm. The fluctuations seen in the compression measurements with both tip sizes were consistent with the expected resolution in force set by a probe spring constant of 0.5 pN/nm and $\sim \pm 5$ nm errors in tracking bead displacements. By comparison, Fig. A2 presents the results for PMN indentation obtained at touch with an ICAM-1 functionalized probe (~ 2.3-μm tip) in Hepes buffer plus 2 mM Mg^{2+}. Here, the linear regression gave a slightly larger stiffness coefficient, $k_{comp} \approx 0.19$ pN/nm.

APPENDIX II: THE INITIAL PMN ELASTIC EXTENSION PLUS SLOW CELL BODY ELONGATION

Shao et al. (1998) employed whole-cell aspiration into a large micropipette to pull PMNs away from attachments to a monoclonal antibody-coated microsphere. With the cell moving freely in the bore of the large pipette, a positive pressure was first applied to initiate PMN contact and then a quick switch to negative pressure was used to pull the cell away. After the switch to negative pressure, a brief period of initial displacement was observed seeming to track the free motion of an unattached cell in the pipette. Then, the cell displacement began to slow and depart from the free motion trajectory, indicating the buildup of an attachment force. We have replotted the sample data from Shao et al. (1998) in Fig. A3 (*left* and *right*). The dotted lines in the figure show the trajectories for free motion of an unattached cell at two suction forces, ~ 34 pN (*left*) and ~ 68 pN (*right*). The free motion velocity is directly proportional to the suction force, implying a constant viscous drag coefficient ($\zeta_{drag} \approx 0.008$ pN s/nm) for the cell movement inside the pipette. The data for positions of the cell lead edge at the lower suction force (Fig. A3, *left*, *open circles*) follow the free motion trajectory up to ~ 300 nm and then exhibit a slow viscoelastic approach to a stationary length of 1 μm. By comparison, the data for the higher suction force (Fig.

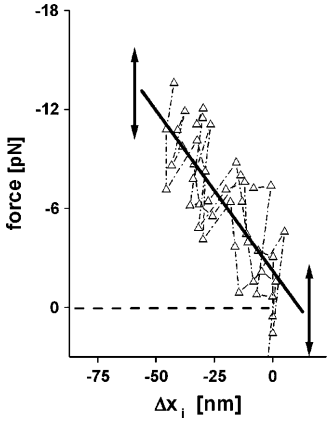

FIGURE A2 Data of force versus PMN indentation distance measured in 2 mM Mg^{2+} during touch to a small diameter probe tip, ~2.3 μm. The indentation stiffness is slightly greater for PMNs in buffer with divalent cations, $k_{comp} = 0.19$ pN/nm. The double-ended arrows illustrate the expected resolution in force set by a probe spring constant of 0.5 pN/nm and ~±5 nm errors in the tracking of bead displacements.

A3, *right*, *open circles*) show an abrupt departure from the free motion trajectory, also at ~300 nm, followed by steady growth of a tether. Finding similar values for the initial free motion displacement, nearly independent of suction force, Shao et al. (1998) concluded that the attachments were formed at the ends of floppy microvilli with ''natural'' lengths of ~300 nm. However, we will show next that our measurements of initial elastic PMN deformation are completely consistent with their observations of the apparent ''free motion'' displacement.

Up to the time of membrane separation and onset of tether flow, we will use a simple model similar to that by Shao et al. (1998) to describe cell deformation. However, we will replace the postulated natural microvillus length by the initial elastic response Δx_i local to the point of contact and the slow viscoelastic elongation postulated to be stretch of the microvillus by a slow cell body ΔD_{PMN} (t) response. Thus, the total displacement is described by, $\Delta D(t) = \Delta x_i$ (t) + ΔD_{PMN} (t). The only subtlety is that the initial elastic response to switching the suction force will be impeded by drag of the cell on the pipette wall. This retardation results in a fast viscoelastic deformation, i.e., $\Delta x_i\,(t) = (f/k_i)\,[1 - \exp(-t/t_\zeta)]$, with a small time constant defined by $t_{drag} = \zeta_{drag} / k_i$. Thus, the total displacement is approximated as a sum of two viscoelastic responses,

$$\Delta D(t) = (f/k_i)[1 - \exp(-t/t_{drag})] + (f/k_D)[1 - \exp(-t/t_D)],$$

where k_D and t_D are the viscoelastic parameters that describe the slow elongation response of the cell body. (The slow cell body relaxation to extensional deformations is well known for PMNs and exhibits time constants similar to t_D; see description and references in Evans and Yeung (1989)). Taking a value for initial elastic stiffness of $k_i \approx 0.2$ pN/nm and the drag coefficient determined from free motion velocity/force ($\zeta_{drag} \approx 0.008$ pN s/nm), the time constant for initial elastic deformation would be, $t_{drag} \approx 0.04$ s. Based on the parameters, k_i and t_{drag}, the solid curve in Fig. A3 (*left*) was fit to the data of Shao et al. (1998), giving an apparent cell-body elastic stiffness $k_D \sim 0.04$ pN/nm and a response time $t_D \sim 0.5$ s. These values are consistent with the values of elasticity (0.043 pN/nm) and characteristic time (0.77 ± 0.35 s) attributed to the stretch response of microvilli in Shao et al. (1998). Modeling the deformation with the same parameters (k_i, t_{drag}, k_D, t_D) up to the point of membrane separation, we see by the solid curve plotted in Fig. A3 (*right*) that the apparent free motion before the onset of tether flow at a force of 68 pN closely agrees with the predicted initial elastic deflection. Clearly, the initial elastic deformation measured in our experiments would lead to a rapid displacement like a constant natural microvillus length when a PMN is first aspirated inside a large pipette while attached at a point, until interrupted by tether formation.

As noted in the text, the slow cell-body extension was not explicitly measured in our experiments. However, we can easily estimate how this added extension affects the apparent value of initial elastic stiffness. In this case, we use the same model of two viscoelastic components in series but with the total elastic deformation growing steadily in time proportional to the pulling speed, i.e. $\Delta D(t) = v_{pull}\,t$. In this case, the damping coefficient for retardation of the initial elastic deformation is the small BFP damping factor, $\zeta_{BFP} \approx 0.0005$ pN s/nm. Likewise, an effective elastic stiffness k_{eff} is needed to characterize the BFP stiffness k_f in series with the initial elastic stiffness, i.e., $k_{eff} = k_i\,/(1 + k_i / k_f)$. This effective stiffness and damping define the time constant for initial elastic deformation, $t_i = \zeta_{BFP} / k_{eff}$, where the combined elastic deformation is, $x_e = f\,(1/k_i + 1/k_f)$. Thus, the dynamic force in each viscoelastic component is equal and defined by,

$$f(t) = k_{eff}[x_e(t) + t_i dx_e/dt] = k_D[\Delta D_{PMN}(t) + t_D\, d\Delta D_{PMN}/dt].$$

Using the kinematic requirement that $\Delta D_{PMN}\,(t) = v_{pull}\,t - x_e(t)$, the solution of a single first-order differential equation predicts the elastic deformation $x_e(t)$ and, thereby, the force is found to be,

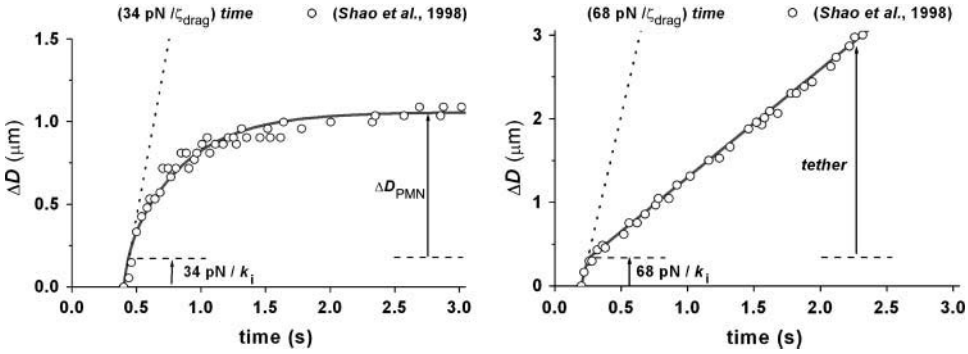

FIGURE A3 Reproduced from Shao et al. (1998), data for PMN displacements inside a large micropipette are shown as a function of time after two different jumps in suction pressure while attached at a point to an antibody-coated bead. Illustrated by dotted lines, the unattached free motion of the cell is characterized by a velocity directly proportional to the suction force, divided by a constant viscous drag coefficient ($\zeta_{drag} \approx 0.008$ pN s/nm). Open circles show the time-dependent advance measured for the cell leading edge, at left pulled by the low suction force (34 pN) and at right pulled by a high suction force (68 pN). With the fast initial deformation response defined by the parameters, $k_i \approx 0.2$ pN/nm and $t_{drag} \approx 0.04$ s, the solid curve in the left panel was the fit to the data based on coupling of the fast response to an apparent slow cell-body elongation described by an elastic stiffness $k_D \sim 0.04$ pN/nm and a response time $t_D \sim 0.5$ s, which are consistent with the values in Shao et al. (1998). Modeling deformation with the same parameters (k_i, t_{drag}, k_D, t_D), the solid curve in the right panel predicts the cell displacement up to the time of membrane separation from the cytoskeleton at ~68 pN, followed by tether flow at constant speed.

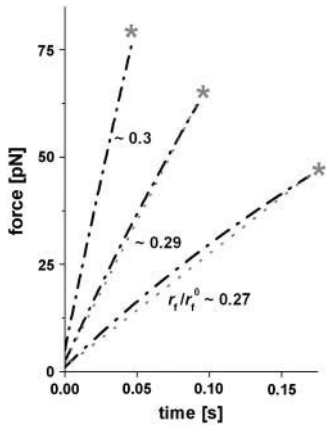

FIGURE A4 Predictions of force versus time for retraction of a PMN from the BFP at fixed speeds (2 μm/s, 4.5 μm/s, 10 μm/s), corresponding to the lowest three loading rates of data in Fig. 7 *B*, i.e., $\langle r_f \rangle \sim 240$ pN/s, 650 pN/s, and 1480 pN/s. The BFP force constant was $k_f = 0.5$ pN/nm. A slow cell-body response described by, $k_D \sim 0.04$–0.05 pN/nm and $t_D \sim 1.2$–1.4 s, was needed to match the loading rates measured in the experiments up to the point of membrane separation (*stars*), accounting for the weak dependence on pulling speed seen in Fig. 5 *A*.

$$f(t) = \alpha\, k_{\text{eff}} v_{\text{pull}} \{(t + t_D) - (t_\alpha - t_i) \times [1 + (t_D/t_\alpha - 1)\exp(-t/t_\alpha)]\},$$

in terms of the following parameters, $\alpha = k_D/(k_D + k_{\text{eff}})$ and $t_\alpha = (1 - \alpha)\, t_i + \alpha\, t_c$.

We have used the dynamic relation for force to model the lowest three loading rates of data appearing in Fig. 7 *B*, i.e., $r_f \sim 240$ pN/s, 650 pN/s, and 1480 pN/s, corresponding to nominal loading rates of $r_f^o = k_f\, v_{\text{pull}} \sim 1000$ pN/s, 2250 pN/s, and 5000 pN/s. For these rates, the BFP force constant was $k_f = 0.5$ pN/nm. The force versus time curves plotted in Fig. A4 represent the force loading up to the membrane unbinding force (*stars*), computed with a fixed initial elastic stiffness $k_i = 0.25$ pN/nm (i.e., $k_{\text{eff}} = 0.167$ pN/nm, $t_i \approx 0.003$ s) and a slow cell-body response described by, $k_D \sim 0.04 - 0.05$ pN/nm and $t_D \sim 1.2$–1.4 s. The viscoelastic parameters for the cell were chosen to exactly match the mean loading rates measured in the experiments and are similar in value to those characterizing the experiments of Shao et al. (1998). The ratios of apparent to nominal loading rates, r_f/r_f^o, shown in Fig. A4 correspond to elastic stiffnesses of 0.18, 0.205, 0.22 pN/nm for the initial cell deformation, accounting for the weak dependence on pulling speed seen in Fig. 5 *A*.

This work was supported by National Institutes of Health grants HL65333 and HL31579.

REFERENCES

Alon, R., S. Chen, K. D. Puri, E. B. Finger, and T. A. Springer. 1997. The kinetics of L-selectin tethers and the mechanics of selectin-mediated rolling. *J. Cell Biol.* 138:1169–1180.

Alon, R., D. A. Hammer, and T. A. Springer. 1995. Lifetime of the P-selectin–carbohydrate bond and its response to tensile force in hydrodynamic flow. *Nature*. 374:539–542.

Bell, G. I. 1978. Models for the specific adhesion of cells to cells. *Science*. 200:618–627.

Božič, B., S. Svetina, B. Žekš, and R. E. Waugh. 1992. The role of lamellar membrane structure in tether formation from bilayer vesicles. *Biophys. J.* 61:963–973.

Brunk, D. K., and D. A. Hammer. 1997. Quantifying rolling adhesion with a cell-free assay. E-selectin and its carbohydrate ligands. *Biophys. J.* 72:2820–2833.

Evans, E., A. Leung, D. Hammer, and S. Simon. 2001. Chemically-distinct transition states govern rapid detachment of single bonds to L-selectin under force. *Proc. Natl. Acad. Sci. USA*. 98:3784–3789.

Evans, E., and K. Ritchie. 1997. Dynamic strength of molecular adhesion bonds. *Biophys. J.* 72:1541–1555.

Evans, E., K. Ritchie, and R. Merkel. 1995. Sensitive force technique to probe molecular adhesion and structural linkages at biological interfaces. *Biophys. J.* 68:2580–2587.

Evans, E., and P. Williams. 2002. Dynamic force spectroscopy: I. single bonds. *In* Physics of Bio-Molecules and Cells. Ecoles des HOUCHES d'Ete LXXV. EDP Sciences, Springer-Verlag, New York. 145 – 185.

Evans, E., and A. Yeung. 1989. Apparent viscosity and cortical tension of blood granulocytes. *Biophys. J.* 56:151–160.

Evans, E., and A. Yeung. 1994. Hidden dynamics in rapid changes of bilayer shape. *Chem. Phys. Lipids*. 73:39–56.

Heinrich, V., B. Božič, S. Svetina, and B. Žekš. 1999. Vesicle deformation by an axial load: from elongated shapes to tethered vesicles. *Biophys. J.* 76:2056–2071.

Heinrich, V., A. Leung, and E. Evans. 2005. Nano- to microscale dynamics of P-selectin detachment from leukocyte interfaces. II. Tether flow terminated by P-selectin dissociation from PSGL-1. *Biophys. J.* 88:2299–2308.

Hochmuth, R. M., J.-Y. Shao, J. Dai, and M. P. Sheetz. 1996. Deformation and flow of membrane into tethers extracted from neuronal growth cones. *Biophys. J.* 70:358–369.

Hwang, W. C., and R. E. Waugh. 1997. Energy of dissociation of lipid bilayer from the membrane skeleton of red blood cells. *Biophys. J.* 72:2669–2678.

Janmey, P. A., U. Euteneuer, P. Traub, and M. Schliwa. 1991. Viscoelastic properties of vimentin compared with other filamentous biopolymer networks. F-actin and F-actin/gelsolin complexes. *J. Cell Biol.* 113:155–160.

Janmey, P. A., S. Hvidt, J. Peetermans, J. Lamb, J. D. Ferry, and T. P. Stossell. 1988. Viscoelasticity of F-actin and F-actin/gelsolin complexes. *Biochemistry*. 27:8218–8227.

Kaplanski, G., C. Famarier, O. Tissot, A. Pierres, A. Benoliel, M. Alessi, S. Kaplanski, and P. Bongrand. 1993. Granulocyte-endothelium initial adhesion. Analysis of transient binding events mediated by E-selectin in laminar shear flow. *Biophys. J.* 64:1922–1933.

King, M. R., V. Heinrich, E. Evans, and D. A. Hammer. 2005. Nano- to microscale dynamics of P-selectin detachment from leukocyte interfaces. III. Numerical simulation of tethering under flow. *Biophys. J.* 88:1676–1683.

Landau, L. D., and E. M. Lifshitz.1986. Theory of Elasticity, Course of Theoretical Physics, Vol. 7. Pergamon Press, Oxford, UK.

Lawrence, M. B., and T. A. Springer. 1991. leukocyte roll on a selectin at physiologic flow rates: distinction from the prerequisite for adhesion through integrins. *Cell*. 65:859–873.

Mangeat, P., C. Roy, and M. Martin. 1999. ERM proteins in cell adhesion and membrane dynamics. *Trends Cell Biol.* 9:187–192.

Marcus, W. D., and R. M. Hochmuth. 2002. Experimental studies of membrane tethers formed from human neutrophils. *Ann. Biomed. Eng.* 30:1273–1280.

McEver, R. P. 2001. Adhesive interactions of leukocytes, platelets, and the vessel wall during hemostasis and inflammation. *Thromb. Haemost.* 86:746–756.

Park, E. Y. H., M. J. Smith, E. S. Stropp, K. R. Snapp, J. A. DiVietro, W. F. Walker, D. W. Schmidtke, S. L. Diamond, and M. B. Lawrence. 2002. Comparison of PSGL-1 microbead and neutrophil rolling: microvillus elongation stabilizes P-selectin bond clusters. *Biophys. J.* 82:1835–1847.

Ramachandran, V., M. Williams, T. Yago, D. W. Schmidtke, and R. P. McEver. 2004. Dynamic alterations of membrane tethers stabilize

leukocyte rolling on P-selectin. *Proc. Natl. Acad. Sci. USA*. 101:13519–13524.

Schmidtke, D. W., and S. L. Diamond. 2000. Direct observation of membrane tethers formed during neutrophil attachment to platelets of P-selectin under physiological flow. *J. Cell Biol.* 149:719–729.

Serrador, J. M., A. Urzainqui, J. L. Alonso-Lebrero, J. R. Cabrero, M. C. Montoya, M. Vicente-Manzanares, M. Yanez-Mo, and F. Sanchez-Madrid. 2002. A juxta-membrane amino acid sequence of P-selectin glycoprotein ligand-1 is involved in moesin binding and ezrin/radixin/moesin-directed targeting at the trailing edge of migrating lymphocytes. *Eur. J. Immunol.* 32:1560–1566.

Shao, J.-Y., H. P. Ting-Beall, and R. M. Hochmuth. 1998. Static and dynamic lengths of neutrophil microvilli. *Proc. Natl. Acad. Sci. USA*. 95:6797–6802.

Simson, D. A., F. Ziemann, M. Strigl, and R. Merkel. 1998. Micropipet-based pico force transducer: in depth analysis and verification. *Biophys. J.* 74:2080–2088.

Snapp, K. R., C. E. Heitzig, and G. S. Kansas. 2002. Attachment of the PSGL-1 cytoplasmic domain to the actin cytoskeleton is essential for leukocyte rolling on P-selectin. *Blood.* 99:4494–4502.

Urzainqui, A., J. M. Serrador, F. Viedma, M. Yanez-Mo, A. Rodriguez, A. L. Corbi, J. L. Alonso-Lebrero, A. Luque, M. Deckert, J. Vazquez, and F. Sanchez-Madrid. 2002. ITAM-based interaction of ERM proteins with Syk mediates signaling by the leukocyte adhesion receptor PSGL-1. *Immunity*. 17:401–412.

Vestweber, D., and J. E. Blanks. 1999. Mechanisms that regulate the function of the selectins and their ligands. *Physiol. Rev.* 79:181–213.